 ©2010 Kvantovaya Elektronika and Turpion Ltd

PACS numbers: 07.85.Fv; 42.65.Re; 52.50.Jm; 52.50.Jm; 52.38.Ph
DOI: 10.1070/QE2010v040n04ABEH014272

Simulation of generation of bremsstrahlung gamma quanta upon irradiation of thin metal films by ultra-intense femtosecond laser pulses

S.N. Andreev, S.G. Garanin, A.A. Rukhadze, V.P. Tarakanov, B.P. Yakutov

Abstract. **We report the results of simulations of generation of bremsstrahlung gamma quanta upon irradiation of a thin-film metal target by ultra-intense femtosecond laser pulses. It is shown by the example of a thin gold target that the mean electron energy is twenty five times higher than the mean energy of gamma quanta generated by them. A simple approximating formula is proposed, which establishes a one-to-one relation between these quantities. The angular distributions of electrons and gamma quanta are studied. It is shown that only the angular distribution of high-energy gamma quanta repeats the angular distribution of the electrons leaving the target.**

Keywords: *bremsstrahlung, laser plasma, PIC-code*.

1. Introduction

Laser plasma produced upon irradiation of a solid-state target by ultra-intense femto-/picosecond laser pulses is a source of hard gamma radiation. Laser-plasma sources of gamma radiation possess unique characteristics (high spectral brightness, micron dimensions of the radiation source, picosecond pulse duration, narrow gamma-radiation directivity) due to which they can be used in such applications as radiography [1], production of short-lived isotopes [2], deactivation of radioactive waste [2, 3], etc. Detailed investigation of the properties of gamma-radiation sources is also required to ensure radiation safety of the personnel working on high-power femto-/picosecond laser facilities [4, 5].

One of the main mechanisms of gamma-quanta generation upon irradiation of solid-state targets by ultra-intense femtosecond laser pulses is the bremsstrahlung of electrons accelerated to the relativistic velocities in the case of their Coulomb scattering from the target nuclei. Different characteristics of the fast-electron bremsstrahlung in laser plasma have been the object of research for a long time because, on the one hand, the experimental methods for detecting gamma quanta are well elaborated and available and, on the other hand, bremsstrahlung contains extensive information on processes proceeding in plasma.

In papers [6 – 10], the fast-electron temperature T_h was determined in laser plasma by the measured power spectrum of bremsstrahlung gamma quanta. For this purpose, the obtained spectral dependences were approximated by the exponential function with the slope of which the corresponding temperatures T_h were calculated in the logarithmic scale. The authors of paper [6] noted however that the slope of the spectral curve significantly changes with increasing the gamma-quanta energy, thus showing a noticeable increase in temperature T_h at higher gamma-quanta energies. This, according to [6], indicates the non-Maxwellian character of the distribution function of the fast electrons over the energies.

It was pointed out in paper [11] that the above procedure for determining the fast-electron temperature in laser plasma is incorrect: the temperature of the bremsstrahlung gamma quanta calculated by the slope of the spectral curve in the logarithmic scale can be significantly smaller than the fast-electron temperature. The authors of [11] also note that the intensity of gamma-quanta radiation has a pronounced angular dependence; therefore, the observation angle of gamma quanta determines their spectrum and, hence, temperature. Thus, extreme caution should be used in determining the angular distribution parameters of incident electrons from the experimentally measured bremsstrahlung spectrum [11].

The angular distribution of the bremsstrahlung gamma quanta in laser plasma significantly depends both on the laser pulse parameters and on the properties of the irradiated target. For example, it was obtained in [11] that in the case of oblique irradiation of a 3-mm-thick lead target by a picosecond laser pulse of intensity 10^{19} W cm^{-2}, the angular distribution of gamma quanta has a maximum in the propagation direction of the laser pulse. It was found in [7] that when a 60-fs laser pulse of intensity 5×10^{18} W cm^{-2} irradiates a 1-mm-thick tantalum target, the bremsstrahlung of weakly relativistic electrons (the gamma-quanta energy does not exceed 0.5 MeV) is almost isotropic and gamma quanta with the energies above 0.5 MeV propagate mainly in the direction of specular reflection of the laser pulse (the angle of incidence of the

S.N. Andreev, A.A. Rukhadze A.M. Prokhorov General Physics Institute, Russian Academy of Sciences, ul. Vavilova 38, 119991 Moscow, Russia; e-mail: andreevsn@ran.gpi.ru, rukh@fpl.gpi.ru;
S.G. Garanin, B.P. Yakutov Research Institute of Laser Physics, Federal State Unitary Enterprise 'Russian Federal Nuclear Center – The All-Russian Research Institute of Experimental Physics', prosp. Mira 37, 607190 Sarov, Nizhnii Novgorod region, Russia;
V.P. Tarakanov Joint Institute for High Temperatures, Russian Academy of Sciences, ul. Izhorskaya 13/19, 127412 Moscow, Russia

Received 23 December 2009; revision received 8 February 2010
Kvantovaya Elektronika **40** (4) 355 – 362 (2010)
Translated by I.A. Ulitkin

laser pulse on the target was 45°). It was determined in paper [4] that in the case of oblique (the angle of incidence is 45°) irradiation of a 10-mm-thick copper target by a 45-fs laser pulse of intensity 1.3×10^{18} W cm^{-2}, the angular distribution of gamma quanta has a maximum in the direction of the normal to the target surface. Analysis of the experimental data allowed the authors of [4] to reveal the presence of two gamma-radiation sources: the first one was on the irradiated surface of the target and the second one, formed by high-energy electron beam, was on the vacuum-chamber wall in the direction of the normal to the target.

To interpret theoretically the experiments on generation of bremsstrahlung gamma quanta during ultra-intense laser pulses interact with matter, many authors (see, for example, [5–7, 11, 12]) used the approach involving two stages. First, they determined {for example with the help of the particle-in-cell (PIC) method [5]} the distribution function of high-energy electrons produced during the interaction of a laser pulse with the target material, which was then used in Monte Carlo simulations describing the electron propagation in the target volume and bremsstrahlung generation. The authors of papers [11, 12] noted that the main disadvantage of this approach is the absence of self-consistency with the electromagnetic field appearing during the propagation of high-energy electrons in the target volume.

Papers [13–15], devoted to the theoretical investigation of gamma-quanta generation during the interaction of ultra-intense femtosecond laser pulses with a solid-state target, employed the PIC-code with an integrated module for calculating the process of bremsstrahlung gamma-quanta generation by the Monte Carlo method.

Paper [13] used the one-dimensional variant of this PIC-code to simulate, in a broad range of intensities, the interaction of laser pulses with carbon films in the case of normal incidence. It was found that gamma quanta with the energy above 100 keV emit strictly in the direction of the laser pulse propagation. At the same time, the azimuth distribution of gamma quanta proves virtually isotropic. Comparison of electron and gamma-quanta spectra at the laser pulse intensity of 2×10^{20} W cm^{-2} showed that the temperature calculated by the gamma-quanta spectrum (1.5 MeV) significantly exceeds the hot-electron temperature (870 keV). Note that this surprising result caused possibly by the model one-dimensionality was not adequately explained in this paper. It was also shown in [13] that at a lower laser pulse intensity (5×10^{18} W cm^{-2}) both temperatures virtually coincide.

The authors of [13] in their next papers [14, 15] studied theoretically the angular distribution of gamma-quanta in the case of oblique incidence of laser radiation on the target by using a two-dimensional variant of the PIC-code developed by them. It was shown that the angular distribution of gamma quanta depends on their energy and correlates substantially with the angular distribution of accelerated electrons. However, the problem of the correlation of the electron and gamma quanta energy spectra was not considered in papers [14, 15] and is essentially open.

This paper is devoted to the numerical investigation of generation of bremsstrahlung gamma quanta upon irradiation of thin-film targets by ultra-intense femtosecond laser pulses. Simulation was performed with the help of a two-dimensional xz version of the relativistic electrodynamic PIC-code KARAT [16] into which a module of bremsstrahlung generation was integrated.

2. Mathematical model of bremsstrahlung generation in the PIC-code KARAT

The mathematical model of the bremsstrahlung generation module in the PIC-code KARAT is based on the results of the relativistic theory of electron–nucleus bremsstrahlung presented in [17, 18].

The expression for the differential cross section $\mathrm{d}\sigma_{\omega\theta}$ of the electron bremsstrahlung with the initial energy E_0 on a nucleus having the charge Z with emission of gamma quanta in the frequency range from ω to $\omega + \mathrm{d}\omega$ at angles in the range from θ to $\theta + \mathrm{d}\theta$ to the initial direction of the electron motion has the form [17]

$$\begin{aligned}
\mathrm{d}\sigma_{\omega\theta} &= \frac{Z^2 \alpha r_e^2}{4} \frac{\mathrm{d}\omega}{\omega} \frac{P_1}{P_0} \sin\theta \mathrm{d}\theta m^2 c^4 \\
&\times \left\{ 8m^2c^4 \sin^2\theta \frac{2E_0^2 + m^2c^4}{P_0^2 c^2 \Delta^4} - \frac{2\left(5E_0^2 + 2E_1E_0 + 3m^2c^4\right)}{P_0^2 c^2 \Delta^2} \right. \\
&- \frac{2\left(P_0^2c^2 - \hbar^2\omega^2\right)}{T^2c^2\Delta^2} + \frac{4E_1}{P_0^2c^2\Delta} + \frac{L}{P_1P_0c^2} \\
&\times \left[\frac{4E_0 \sin^2\theta m^2c^4 \left(3\hbar\omega m^2c^4 - P_0^2c^2E_1\right)}{P_0^2c^2\Delta^4} \right. \\
&+ \frac{4E_0^2\left(E_0^2 + E_1^2\right) - 2m^2c^4\left(7E_0^2 - 3E_1E_0 + E_1^2\right) + 2m^4c^8}{P_0^2c^2\Delta^2} \\
&\left. + 2\hbar\omega \frac{E_0^2 + E_1E_0 - m^2c^4}{P_0^2c^2\Delta} \right] + \frac{\tilde{l}_1}{P_1c^2T} \\
&\left. \times \left(\frac{4m^2c^4}{\Delta^2} - \frac{6\hbar\omega}{\Delta} - 2\hbar\omega \frac{P_0^2c^2 - \hbar^2\omega^2}{T^2c^2\Delta} \right) - \frac{4l_1}{P_1c\Delta} \right\}, \quad (1)
\end{aligned}$$

where m is the electron mass; c is the speed of light; $\hbar$ is Planck's constant; $\alpha = e^2/(\hbar c)$ is the fine-structure constant; e is the electron charge; $r_e = e^2/(mc^2)$ is the classical radius of an electron; $E_1 = E_0 - E_\gamma$ is the scattered electron energy; $E_\gamma = \hbar\omega$ is the gamma-quanta energy; momentums of incident ($\boldsymbol{P}_0$) and scattered ($\boldsymbol{P}_1$) electrons are related with their energies by the expressions

$$E_0^2 = P_0^2c^2 + m^2c^4, \quad E_1^2 = P_1^2c^2 + m^2c^4. \quad (2)$$

In addition, the following notations are used in (1)

$$\begin{aligned}
&\Delta = E_0 - P_0c\cos\theta; \quad T^2c^2 = P_0^2c^2 - 2P_0c\hbar\omega\cos\theta + \hbar^2\omega^2; \\
&L = \ln\left(\frac{E_1E_0 - m^2c^4 + P_1P_0c^2}{E_1E_0 - m^2c^4 - P_1P_0c^2}\right); \; l_0 = \ln\left(\frac{E_0 + P_0c}{E_0 - P_0c}\right); \quad (3) \\
&l_1 = \ln\left(\frac{E_1 + P_1c}{E_1 - P_1c}\right); \quad \tilde{l}_1 = \ln\left(\frac{Tc + P_1c}{Tc - P_1c}\right).
\end{aligned}$$

Integration in expression (1) over the angle θ in the range $0 - \pi$ leads to the following expression for the spectral distribution of the differential cross section of bremsstrahlung ([18], § 93):

$$\mathrm{d}\sigma_\omega = Z^2\alpha r_e^2 \frac{\mathrm{d}\omega}{\omega} \frac{P_1}{P_0} \left[\frac{4}{3} - 2E_0E_1 \frac{P_1^2c^2 + P_0^2c^2}{P_0^2c^2P_1^2c^2} + \right.$$

$$+m^2c^4\left(l_0\frac{E_1}{P_0^3c^3}+l_1\frac{E_0}{P_1^3c^3}-l_0l_1\frac{1}{P_0P_1c^2}\right)+LF\Bigg],$$

$$F=\Bigg[\frac{8E_0E_1}{3P_0P_1c^2}+\frac{\hbar^2\omega^2}{P_0^3P_1^3c^6}\left(E_0^2E_1^2+P_0^2P_1^2c^4+m^2c^4E_0E_1\right) \tag{4}$$

$$+\frac{m^2c^4\hbar\omega}{2P_0P_1c^2}\left(l_0\frac{E_0E_1+P_0^2c^2}{P_0^3c^3}-l_1\frac{E_0E_1+P_1^2c^2}{P_1^3c^3}\right)\Bigg].$$

The admissible values of gamma-quanta frequencies in expressions (1) and (4) are limited by the condition $Ze^2/(\hbar V_1)\ll 1$ imposed on the electron velocity V_1: the electron should not lose almost all its energy (note that at $V_1=e^2/\hbar$ the kinetic energy of an electron is equal to the hydrogen-atom ionisation potential of 13.6 eV).

At the frequency $\omega\to 0$, the radiation cross section diverges proportionally to $d\omega/\omega$, which is manifestation of the general rule, the so-called infrared catastrophe. In this case, expressions (1) and (4) obtained based on the perturbation theory prove inapplicable. A more adequate approach at small ω, which takes into account emission of 'soft' photons, is not used in the present version of the gamma-quanta generation module. Instead of it, the minimal frequency of gamma quanta generated in the KARAT code as well as the minimal energy of electrons emitting gamma quanta are set. By default, the minimal value of ω corresponds to the energy $E_{\gamma\min}=\hbar\omega_{\min}=1.23$ keV and the minimal kinetic energy $K_{0\min}$ of electrons emitting gamma quanta is chosen equal to 100 keV.

The gamma-quanta generation module operates by using the following algorithm. At each time step for each macroparticle corresponding to an electron, we calculate the probability of gamma-quanta generation event $W=\sigma V_0 n_i$, where $\sigma(E_0)=\int_{\omega_{\min}}^{E_0/\hbar}d\sigma_\omega$ is the total cross section of electron bremsstrahlung with the energy E_0; $V_0=c[1-(mc^2/E_0)^2]^{1/2}$ is the velocity of the given electron; n_i is the ion concentration in the simulated plasma at the location point of the given electron at a given instant. Then, the calculated probability is compared with a random number χ from the interval 0–1; if it is smaller than this number, we pass to the next electron. Otherwise, the procedure of gamma-quanta generation is launched at the location point of the given electron.

The angle at which a gamma quantum is emitted in the plane perpendicular to the initial electron momentum, is assumed uniformly distributed in the range $0-2\pi$ [13]. Therefore, when a gamma quantum is produced, it is sufficient to determine its energy and the exit angle θ with respect to the momentum of the initial electron. The gamma-quantum frequency ω at the given energy E_0 of the incident electron is determined from the integral equation

$$\int_{\omega_{\min}}^{\omega}d\sigma_\omega\sigma^{-1}(E_0)=\chi_1,$$

where χ_1 is a random number from the range 0–1. Finally, the exit angle θ at the given E_0 and $\hbar\omega$ is found from the integral equation

$$\int_0^{\theta}d\sigma_{\omega\theta'}\Big/\int_0^{\pi}d\sigma_{\omega\theta'}=\chi_2,$$

in which χ_2 is a random number from the range 0–1.

After the gamma quantum is emitted, we calculate its motion before arrival to the boundary of the simulation region, where its parameters are fixed. Because, the gamma-quantum generation event is unlikely and does not influence the plasma energy balance, a simplified model is used for an incident electron in which it, after emitting a gamma quantum with the energy E_γ, keeps on moving in the same direction but with the energy reduced by E_γ.

Note that the KARAT code provides a possibility for artificially increasing the generation probability of bremsstrahlung gamma quanta by introducing an additional multiplier to expressions (1) and (4).

3. Simulation of generation of bremsstrahlung gamma quanta during the interaction of a monoenergetic electron beam with a plasma target

It is convenient to test the gamma-quanta generation module when the monoenergetic electron beam interacts with an immobile plasma target. Because the initial vectors of the velocities of all the electrons in the beam are identical, the energy spectrum of gamma quanta appearing when the electrons in the beam are scattered from the plasma target, should be proportional to differential scattering cross section (4), while the angular distribution of gamma quanta should be proportional to scattering cross section (1) integrated over its entire frequency range ω.

The beam of monoenergetic electrons was directed from the left boundary of the simulation region of size 30×30 cm (along the x and z axes, respectively) on the plasma target of size 6×10 cm consisting of electrons and protons with the concentration 2×10^{11} cm^{-2}. We used the multiplier 10^7 in expressions (1) and (4) to increase artificially the gamma-quanta generation probability.

Figure 1 shows the interaction of a beam of electrons with the kinetic energy $K_0=E_0-mc^2=5$ MeV with the plasma target. One can see that gamma quanta fly apart at a relatively narrow angle along the direction of the electron-beam propagation, which corresponds to the ultra-relativistic case ($K_0\gg mc^2$).

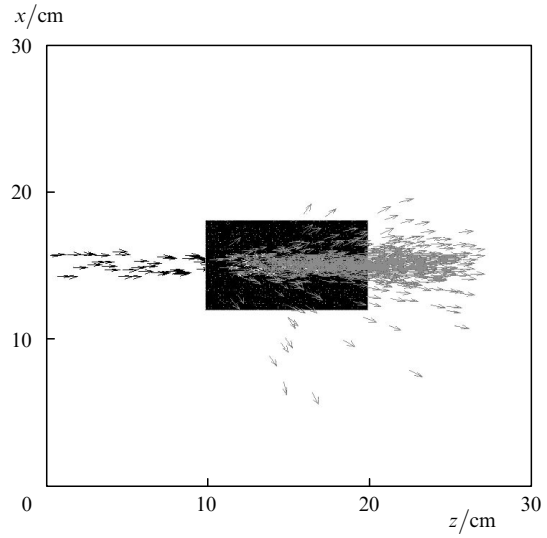

Figure 1. Picture of the electron-beam (black arrows) – plasma-target interaction. Grey arrows show gamma quanta.

Figure 2 presents energy spectra of gamma quanta incident on the right boundary of the simulation region at different initial kinetic electron energies K_0 as well as their corresponding dependences of scattering cross sections on the gamma-quantum energy calculated with the help of expression (4). One can see that the energy spectra coincide with similar curves in the entire range of gamma-quanta energies, except the energy near K_0 at which the electron transfers almost all its energy to the gamma quantum.

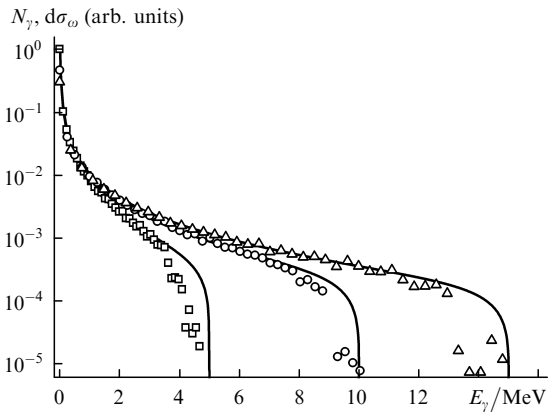

Figure 2. Energy spectra of gamma quanta at initial kinetic electron energies $K_0 = 5$ (□), 10 (○), and 15 MeV (△), as well as the corresponding dependences of scattering cross sections $d\sigma_\omega$ on the gamma-quanta energy calculated by using expression (4) (solid curves); N_γ is the number of gamma quanta.

It follows from calculations that the average energy $\langle E_\gamma \rangle$ of gamma quanta incident on the right boundary of the simulation region is significantly lower than the electron energy E_0. By using expression (4) we can calculate the average-over-spectrum energy of a gamma quantum emitted by an electron with the energy E_0:

$$\langle E_\gamma \rangle = \int_{\omega_{\min}}^{E_0/\hbar} \hbar\omega d\sigma_\omega \Big/ \int_{\omega_{\min}}^{E_0/\hbar} d\sigma_\omega, \qquad (5)$$

which is obviously independent of the nuclear charge Z. The quantity $\langle E_\gamma \rangle$ calculated by expression (5) depends on the choice of the minimal gamma-quantum energy $E_{\gamma\min}$. When using by default the energy $E_{\gamma\min} = 1.23$ keV in the KARAT code, expression (5) well approximates in the energy range 0.01 MeV $\leqslant K_0 \leqslant$ 10 MeV by the expression:

$$\langle E_\gamma \rangle = 0.039K_0 + 0.016, \qquad (6)$$

where $\langle E_\gamma \rangle$ and K_0 are taken in MeV.

Figure 3 demonstrates the dependences $\langle E_\gamma \rangle$ on K_0 at different $E_{\gamma\min}$. One can see that the simulation results are well described by curve (*1*). Note also that the influence of the choice of $E_{\gamma\min}$ on $\langle E_\gamma \rangle$ is insignificant: when $E_{\gamma\min}$ is increased by 100 times, the energy $\langle E_\gamma \rangle$ increases not more than by 2.5 times.

Figure 4 shows the dependences of scattering cross section (1) integrated over ω on the angle θ and the corresponding angular distributions of gamma quanta incident on the right boundary of the simulation region at different K_0. One can see that the calculation results

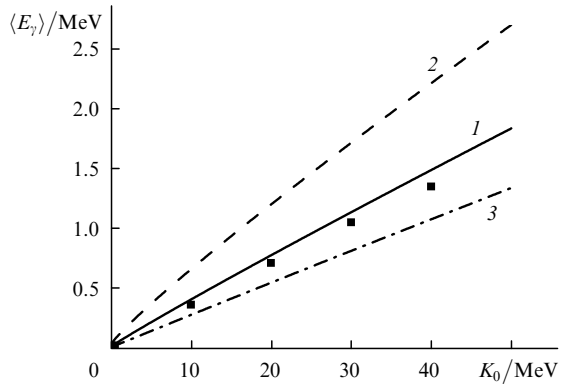

Figure 3. Dependences of the average gamma-quanta energy $\langle E_\gamma \rangle$ on the kinetic electron energy K_0 at $E_{\gamma\min} = 1.23$ (*1*), 12.3 (*2*), and 0.12 keV (*3*). Points are the average energy of gamma quanta incident on the right boundary of the simulation region at $E_{\gamma\min} = 1.23$ keV.

rather well coincide with theoretical curves in the angle range $\theta < 45^\circ$. The discrepancy of the dependences at larger angles is explained by the fact that in constructing the angular distribution we took into account only the gamma quanta incident on the right boundary of the simulation region.

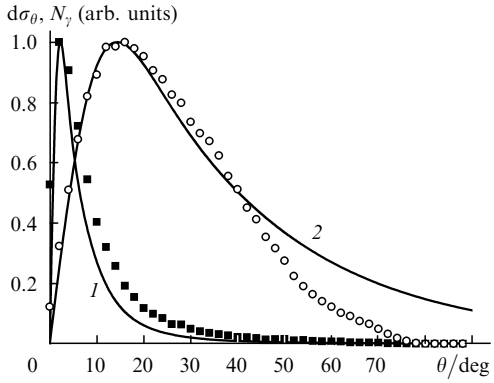

Figure 4. Dependences of the scattering cross sections $d\sigma_\theta$ (solid curves) and the number of gamma quanta N_γ (points) incident on the right boundary of the simulation region on the angle θ at $K_0 = 5$ MeV (*1*, ■) and 500 keV (*2*, ○).

Figure 5 presents the dependence of the angle θ_{ext}, corresponding to the maximum of the angular distribution of gamma quanta, on the kinetic incident-electron energy K_0 calculated from expression (1). One can see that the angle between the directions of the incident-electron motion and the maximum of the angular gamma-quanta distribution decreases with increasing the kinetic incident-electron energy and tends to zero, proportionally to K_0^{-1} in the ultra-relativistic limit.

4. Simulation of generation of bremsstrahlung gamma quanta upon irradiation of gold foil by a femtosecond laser pulse

The simulation region was a 30 × 30-μm rectangle along the x and z axes, respectively. In both directions, the mesh size was 43 nm. The total duration of each simulation t_f was 1 ps.

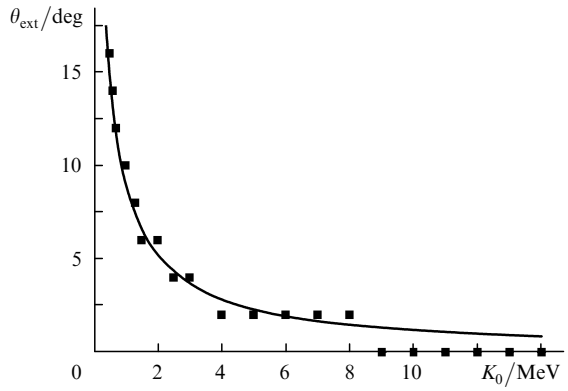

Figure 5. Calculated (points) and analytic (solid curve) dependences of the angle θ_{ext} corresponding to the maximum of the angular gamma-quanta distribution on the kinetic energy K_0 of the incident electron.

70-fs, 0.91-μm laser pulses with the intensity of $I_0 = 10^{21}$ W cm^{-2} had a Gaussian profile both in time and space with a spot size $r_0 = 5$ μm with respect to half an amplitude with a centre at point $x = 15$ μm. The pulse was 'started up' from the left boundary of the simulation region and propagated in the positive direction of the z axis, the electric field of the laser pulse lying in the xz plane. The laser pulse maximum reached the target surface at the instant $t = 150$ fs.

The boundary conditions for electric and magnetic fields on the left (input) and lower (output) boundaries of the simulation region corresponded to the open boundary ensuring radiation transfer. On other boundaries of the simulation region, the boundary conditions corresponded to the conditions on a perfectly conducting surface. All the boundaries of the simulation region for macroparticles were absorbing.

The target was a gold foil ($Z = 79$) of thickness 0.5 μm and length 28 μm with a centre at a point with the coordinates $x = 15$ μm and $z = 15$ μm, rotated by 45° with respect to the direction of the laser pulse propagation. The target was simulated in the form of a singly ionised collisionless plasma consisting of electrons and gold ions Au^+ with the concentration $n_i = 5.87 \times 10^{22}$ cm^{-3} corresponding to the solid-state density of gold. It is obvious, however, that multiply ionised atoms will be also produced at the laser pulse intensity $I_0 = 10^{21}$ W cm^{-2} in a real experiment. The problem of the influence of the ionisation degree of the target atoms on the simulation results is considered below.

In the gamma-quantum generation module, the minimal value of ω corresponded to the energy $E_{\gamma\min} = 1.23$ keV, and the minimal kinetic energy $K_{0\min}$ of electrons emitting gamma quanta was chosen equal to 100 keV.

We determined the relation between the average enegies of the electrons and gamma quanta generated by these electrons at some fixed time by performing the averaging over the electrons with the energy $K > K_{0\min}$ and all the gamma quanta residing in the region occupied by the target (more rigorously – occupied by the gold ions, because the gamma-quanta generation is possible only in the region where the density of gold ions is non-zero).

Figure 6 shows the time dependence of the average kinetic electron energy $\langle K \rangle$ [curve (*1*)] and the average gamma-quanta energy $\langle E_\gamma \rangle$ (points) in the region occupied by the target. The theoretical time dependence of the energy $\langle E_\gamma \rangle$ [curve (*2*)] was obtained from curve (*1*) by recalculating expression (5). One can see that curve (*2*) describes with good accuracy the behaviour of the average gamma-quanta energy. Thus, expression (5) [and approximating relation (6)] establish one-to-one correlation between the average energies of the electrons and gamma quanta generated by these electrons and can be used to express one quantity by another one. It follows from Fig. 6 that the average gamma-quanta energy is approximately 25 times smaller than the average electron energy. This result agrees with the assertion made in paper [11] that the bremsstrahlung gamma-quanta temperature can be significantly smaller than the fast-electron temperature.

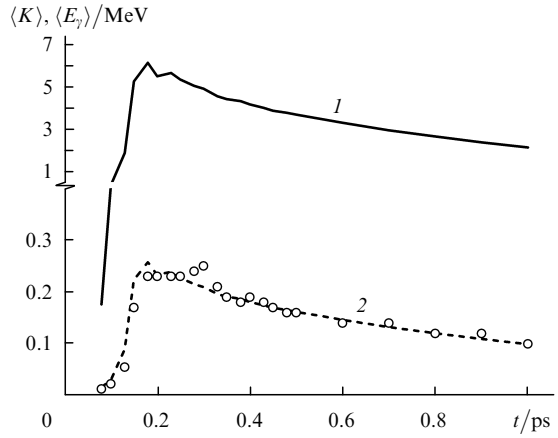

Figure 6. Time dependences of the average energies of the electrons $\langle K \rangle$ (*1*) and gamma quanta $\langle E_\gamma \rangle$ generated by these electrons (○). Curve (*2*) is obtained from curve (*1*) by recalculating expression (5).

Note that expressions (5) and (6) well describe the relation between the average energies of the electrons and gamma quanta generated by these electrons in a wide range of the laser pulse intensities. Thus, for example, at the intensity $I_0 = 10^{19}$ W cm^{-2}, the results of calculations show that at the instant $t = 150$ fs the average kinetic electron energy with $K > K_{0\min}$ is 415 keV. Using expression (6), we will calculate the average gamma-quanta energy that proves equal to 31 keV, which satisfactorily agrees with the value of 24 keV obtained in calculations.

Consider now the problem of the angular distribution of electrons and gamma quanta generated by them. In calculating the angular distributions we determined the number of particles incident on the 6-μm-long segment of the simulation region boundary whose centre is located at a given angle to the direction of the laser pulse incidence relative to the target centre.

Figure 7 presents the angular distributions of the electrons, which reached the simulation region within 500 fs and 1 ps. One can see that these distributions have two pronounced maxima – in the direction of the laser pulse incidence (180°) and in the direction (259°) close to the direction of specular reflection of laser radiation from the target. The presence of the first maximum is caused by acceleration of the target electrons in the direction of the laser pulse incidence under the action of $\boldsymbol{V} \times \boldsymbol{B}$ component of the Lorentz force, which becomes determining at the laser pulse intensitites $\sim 10^{21}$ W cm^{-2}. The existence of the second maximum was substantiated in paper [19] and

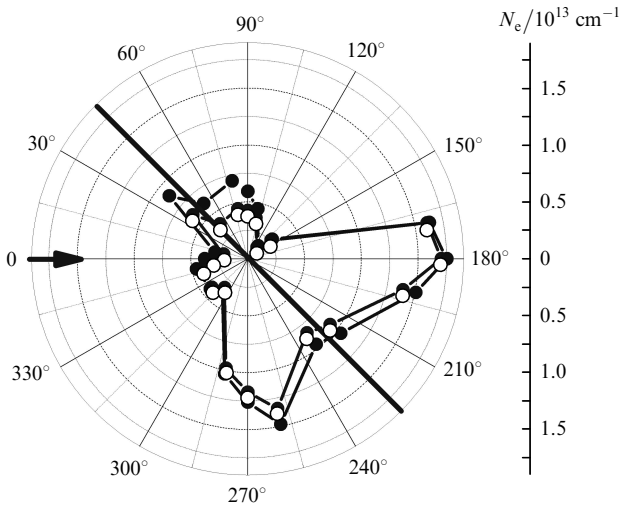

Figure 7. Angular distributions of the electrons reaching the boundary of the simulation region within 500 fs (○) and 1 ps (●). The arrow shows the direction of the laser pulse propagation and the straight line located at an angle of 45°, – the target position (N_e is the number of electrons).

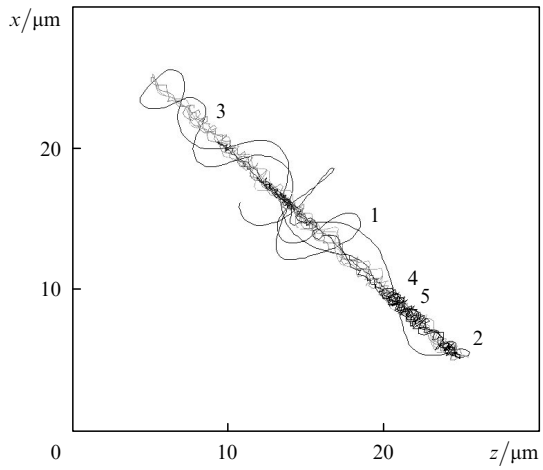

Figure 8. Trajectories of five probe electrons (1 – 5) of the target within 500 fs.

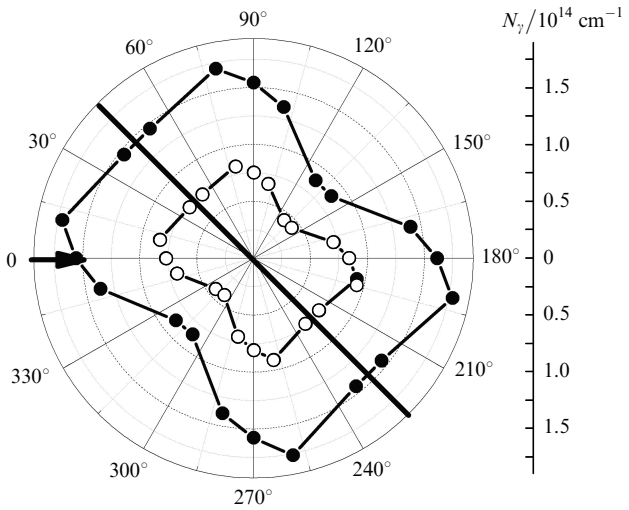

Figure 9. Angular distributions of the gamma quanta reaching the boundary of the simulation region within 500 fs (○) and 1 ps (●). The arrow shows the direction of the laser pulse propagation and the straight line located at an angle of 45°, – the target position.

confirmed in many experimental papers (see, for example, [20, 21]). The authos of paper [19] point out, in particular, that '... only ultrarelativistic electrons escape from the target in the direction close to the specular reflection direction'.

Note that the curves in Fig. 7 slightly differ from each other despite the fact that the time intervals during which the particles were accumulated on the segments of the simulation region boundary differ twice. This means that the high-energy electrons can leave the target and reach the boundary of the simulation region mainly within the first 500 fs (in fact, during the action of the laser pulse on the target). Within the next 500 fs, only a small number of the electrons reach the simulation region boundary, while the majority of them stay near the target; their average energy decreasing rather slowly (Fig. 6).

Figure 8 shows the trajectories (within the first 500 fs) of five probe electrons accelerated by the laser pulse up to different kinetic energies: electron 5 had the minimal energy of 1.5 MeV, while electron 1 had the maximum energy of 48 MeV. One can see that the electron motion represents a superposition of vibrational and translational motions along the target. The trajectories of these electrons fill almost the entire volume of the target. Frequently changing the direction while moving along the target, the electron has a probability of emitting gamma quanta in an arbitrary direction. For this reason, the angular gamma-quanta distribution can significantly differ from the angular electron distribution presented in Fig. 7.

Figure 9 presents the angular distributions of gamma quanta, which reached the simulation region boundary within 500 fs and 1 ps. One can see that these distributions are almost symmetric, their maxima being located at the angles 11°, 79°, 191°, and 259°. The two first maxima reside close to the initial direction of laser radiation propagation and the direction of its specular reflection from the target, respectively, and correlate with the maxima of the angular distributions of the fast electrons. As was pointed out above, the maxima of the angular gamma-quanta distribution in these directions were observed in experiments, for example, in papers [7, 11].

Comparison of the curves in Fig. 9 shows that the angular gamma-quanta distribution, obtained within the first 500 fs, almost does not change its shape within the next 500 fs within which the number of gamma quanta reaching the simulation region boundary increases twice. This is explained by the fact that the majority of gamma quanta are generated by relatively low-energy electrons which do not leave the target during the entire calculation time. Indeed, the average energy of gamma quanta reaching the simulation region boundary within 1 ps is 186 keV, which correspond the average electron energy of 4.4 MeV [see expression (6)]. The trajectory of probe electron 3 with the average energy of ~ 4 MeV (Fig. 8) is such that this electron stays within the target.

High-energy gamma quanta generated by the electrons leaving the simulation region have angular distributions corresponding to a greater extent to the electron distributions presented in Fig. 7. Indeed, Fig. 10 demonstrates the angular distributions of high-energy gamma quanta reaching the simulation region boundary within 500 fs at different E_γ. One can see that the both curves are not symmetric as

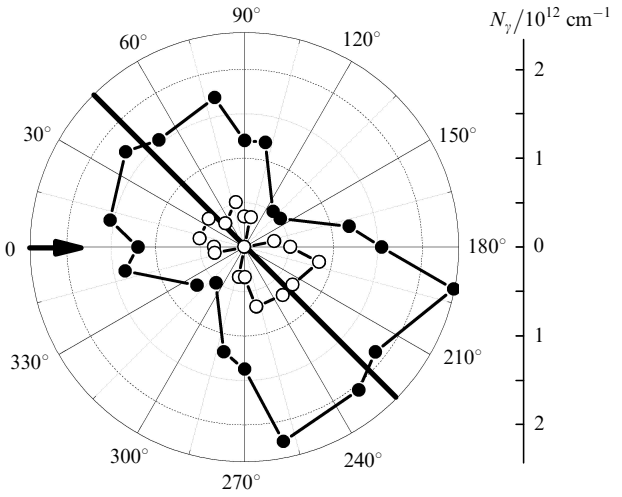

Figure 10. Angular distributions of the high-energy gamma quanta reaching the boundary of the simulation region within 500 fs at $E_\gamma >$ 0.89 MeV (●) and $E_\gamma > 2.67$ MeV (○). The arrow shows the direction of the laser pulse propagation and the straight line located at an angle of 45°, – the target position.

would be the case in Fig. 9. The maxima of the angular distributions are located at the angles of 191° and 259°, in agreement with the directions of the maxima in Fig. 7.

Thus, the angular distribution of gamma quanta differs substantially from that of electrons. However, in the case of high-energy electrons and gamma quanta, their angular distributions repeat each other.

In conclusion, we will estimate the ionisation degree of gold atoms on the target surface by using the model developed in paper [22] for tunnel ionisation of the atomic ion in a laser field. According to this model, the probability of tunnel ionisation of the atomic ion will be close to unity if its ionisation potential satisies the relation:

$$U_N \leqslant U_{\mathrm{H}} \left(\frac{3}{2} \frac{\mathscr{E}_{\max}}{\mathscr{E}_{\mathrm{a}}} \right)^{2/3}, \qquad (7)$$

where U_N is the Nth ionisation potential of the atomic ion; $U_{\mathrm{H}} = 13.6$ eV is the ionisation potential of the hydrogen atom; $\mathscr{E}_{\mathrm{a}} = 5.14 \times 10^9$ V cm^{-1} is the atomic unit of the electric field strength. According to the calculations, in the case of the laser pulse action with the intensity $I_0 = 10^{21}$ W cm^{-2}, the maximum electric-field amplitude $\mathscr{E}_{\max}$ on the frontal surface of the target achieves $\sim 10^{12}$ V cm^{-1}. By substituting the value $\mathscr{E}_{\max}$ into expression (7), we obtain $U_N = 598$ eV, which corresponds to the gold atom with the ionisation degree 22 (the potential $U_{22} = 587.1$ eV for gold is calculated by the mean-ion method [23]). The exact values of the ionisation degree of the target atoms as well as the distributions of the electron density in the target can be obtained in simulating the interaction of the laser pulse with the target taking into account the ionisation kinetics, which is beyond the framework of the present research. Nevertheless, we will consider the problem of the influence of the ionisation degree of gold ions on the average energies of the electrons and gamma quanta generated by these electrons under assumption that the ionisation degree N is the same for all the target ions and does not change in time, while the distribution of the electrons and ions across the target is uniform at the initial instant.

Figure 11 shows the dependences of the maximal average energy of electrons [curve (*1*)] and the average energy of gamma quanta generated by these electrons [curve (*2*)] on the ionisation degree N. The theoretical dependence of the average gamma-quanta energy [curve (*3*)] obtained from curve (*1*) by recalculating expression (6), well correspond to curve (*2*) (the discrepancy is less than 20 %). One can see that when the ionisation degree increases, the average energies of the electrons and gamma quanta decrease starting saturation at $N > 5$. This is explained by a decrease in the absorption length of the laser pulse in the target and, hence, by a decrease in the region of radiation – electron interaction with increasing the ionisation degree of plasma. In this case, the relative number of accelerated electrons and their average energy decrease. The processes of multiple ionisation in relativistic laser plasma will be studied in detail elsewhere.

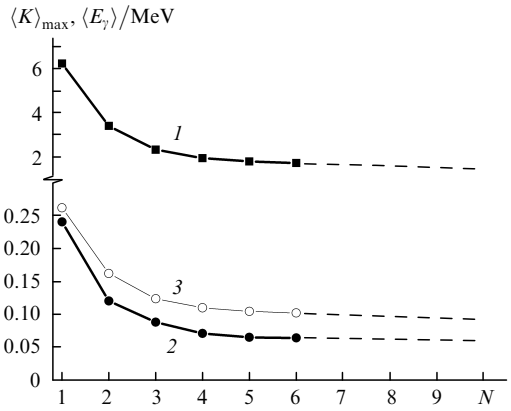

Figure 11. Dependences of the maximum average energy of the electrons $\langle K \rangle_{\max}$ (*1*) and the average energy of the gamma quanta generated by these electrons $\langle E_\gamma \rangle$ (*2*) on the ionisation degree N of the target atoms. Curve (*3*) was obtained from curve (*1*) by recalculating expression (6). Dashed curves show extrapolation of the curves in the region of larger N.

5. Conclusions

We have simulated the generation of bremsstrahlung gamma quanta in the case of oblique incidence of ultra-intense femtosecond laser pulse on a thin-film gold target. Simulation has been performed by using a two-dimensional xz version of the relativistic electrodynamic PIC-code KARAT with the bremsstrahlung generation module. It is shown that in the case of the thin-film target, the gamma-quanta energy is twenty five times smaller than the average energy of the electrons. We have proposed simple approximating expression (6) establishing a one-to-one relation between these energies.

We have studied the angular distributions of the electrons and gamma quanta, which reached the simulation region boundaries. It has been found that the angular distributions of the high-energy electrons leaving the target have two maxima – in the directions of the incidence of the laser pulse on the target and in the direction of its specular reflection. Unlike the electrons, the angular gamma-quanta distribution is symmetric. This is caused by the fact that many gamma quanta are generated by relatively low-energy electrons, which do not leave the target during the calcu-

lation time. Frequently changing the direction when moving along the target, these electrons have a probability of emitting gamma quanta in different directions. However, in the case of high-energy electrons leaving the target and in the case of high-energy gamma quanta generated by these electrons, their angular distributions repeat each other.

We have estimated the probable ionisation degree of target atoms for the laser interaction parameters under study. We have shown that when the ionisation degree of the target atoms increases, the average energies of the electrons and gamma quanta generated by these electrons significantly decrease.

Acknowledgements. The authors thank V.P. Makarov for useful discussions of the results of the paper and valuable remarks.

References

1. Edwards R.D. et al. *Appl. Phys. Lett*., **80**, 2129 (2002).
2. Ewald F. et al. *Plasma Phys. Control. Fusion A*, **45**, 83 (2003).
3. Ledingham K.W.D. et al. *J. Phys. D: Appl. Phys*., **36**, L79 (2003).
4. Rao B.S., Naik P.A., Arora V., Khan R.A., Gupta P.D. *J. Appl. Phys*., **102**, 063307 (2007).
5. Courtois C. et al. *Phys. Plasmas*, **16**, 013105 (2009).
6. Key M.H. et al. *Phys. Plasmas*, **5**, 1966 (1998).
7. Schwoerer H., Gibbon P., Dusterer S., Behrens R., Ziener C., Reich C., Sauerbrey R. *Phys. Rev. Lett*., **86**, 2317 (2001).
8. Chen L.M. et al. *Phys. Plasmas*, **11**, 4439 (2004).
9. Bol'shakov V.V., Vorob'ev A.A., Uryupina D.S., Ivanov K.A., Morshedian N., Volkov R.V., Savel'ev A.B. *Kvantovaya Elektron*., **39**, 669 (2009) [*Quantum Electron*., **39**, 669 (2009)].
10. Belyaev V.S. et al. *Yad. Fiz*., **71**, 466 (2008).
11. Norreys P.A. et al. *Phys. Plasmas*, **6**, 2150 (1999).
12. Hatchett S.P. et al. *Phys. Plasmas*, **7**, 2076 (2000).
13. Sentoku Y., Mima K., Taguchi T., Miyamoto S., Kishimoto Y. *Phys. Plasmas*, **5**, 4366 (1998).
14. Sentoku Y., Ruhl H., Mima K., Kodama R., Tanaka K.A., Kishimoto Y. *Phys. Plasmas*, **6**, 2855 (1999).
15. Sheng Z.M., Sentoku Y., Mima K., Zhang J., Yu W., Meyer-ter-Vehn J. *Phys. Rev. Lett*., **85**, 5340 (2000).
16. Tarakanov V.P. *User's Manual for Code KARAT* (Springfield, VA, USA: Berkeley Research Associates, 1992).
17. Gluckstern R.L., Hull M.H. *Phys. Rev*., **90**, 1030 (1953).
18. Berestetskii V.B., Lifshits E.M., Pitaevskii L.P. *Quantum Electrodynamics* Oxford: Butterworth-Heinemann, 1999; Moscow: Nauka, 1980).
19. Ruhl H., Sentoku Y., Mima K., Tanaka K.A., Kodama R. *Phys. Rev. Lett*., **82**, 743 (1999).
20. Cai D.F. et al. *Phys. Plasmas*, **10**, 3265 (2003).
21. Li Z. et al. *Phys. Plasmas*, **13**, 043104 (2006).
22. Perelomov A.M., Popov V.S., Terent'ev M.V. *Zh. Eksp. Teor. Fiz*., **50**, 1393 (1965).
23. Bel'kov S.A., Gasparyan P.D., Kochubei Yu.K., Mitrofanov E.I. *Zh. Eksp. Teor. Fiz*. **111**, 496 (1997).